Chapter 3: Materials and Methodology

To understand how an experiment/ simulation is conducted, a materials and methodology section is required to promote transparency and reproducibility to replicate the experiment. In this regard, this chapter discusses the materials and methodology adopted for the present work. It has been categorised into four sections. First section includes the materials and methodology adopted for the gasification-engine experimental investigation. This section includes all the technical details of the equipment used while performing experimental work. Second section incorporates the economic analysis of briquetting system and gasification-engine power system to evaluate the financial viability of producing briquettes from sugarcane bagasse pith residues for waste-to-fuel analysis and decentralized power generation analysis. Third section includes the Quasi-dimensional thermodynamic modelling approach and the methodology adopted to perform the simulation work for SI engine. Last section includes the methodology adopted to perform the RSM based multi-objective optimization analysis. This section also includes the block diagram and the flowchart to obtain optimized parameters.

3.1 Experimental Methodology

3.1.1 Experimental setup

For experimenting, the low-grade coal, waste biomass (mahua wood, coconut shell, briquette) feedstocks for downdraft gasifier, were collected from nearby areas in Varanasi, Uttar Pradesh, India. The coal used to arrive from Bihar and Madhya Pradesh mines, and the mahua wood, coconut shell came from the local forest of Gorakhpur and Jaunpur districts of Uttar Pradesh.

The gasifier- internal combustion engine (ICE) experimental design includes a downdraft gasification system with a blower, thermocouple integration, cyclone separator, scrubber, air

control valve, test flare, and three-chambered exemplary filtering system, a compression ignition (CI) engine, and a water pump. The gasifier-IC engine setup is depicted schematically in Figure 3.1.1. For calculating the brake power (BP) of the engine, brake dynamometer device has been used to determine the torque and angular speed of the engine output shaft. In order to provide load to the engine, the engine was fastened to a test bed, and the shaft was coupled to an eddy current dynamometer via a propeller shaft. Eddy current dynamometer contains a stator and a rotor disc and it is coupled to the engine's output shaft. A crank angle sensor is mounted at the crankshaft's end to measure the RPM of an engine. Engine management systems (Engine soft) employ this data to regulate the timing of the ignition system, fuel injection, and other engine characteristics. A thick mild steel batch-type air-based downdraft fixed-bed Gasifier with self-heating measures 73 cm in dia. and 200 cm in height. The reactor includes cleaning (water-based), separation (cyclonic), and filtration, permitting producing gas to flow through. The PG was then subjected to a series of checkpoints to confirm its flammability till the checking fire became a different colour and blazed. To effectively separate impurities, producer gas was made to pass in a sinusoidal waveform through a three-chamber filtration unit, firstly via a fine filter, then via a fabric filter media made of rice husk, wood dust, and cotton cloth. The modifications required to IC engine application may vary based on the specific characteristics of the biomass gasification system, the PG produced, and the type of engine being used. A dual-fuel system can be incorporated that allow the engine to run on both PG and conventional fuels. This provides flexibility in case PG availability or quality varies. In the current experimental work, the filtered PG is connected to the inlet manifold of the CI engine via T-joint inlet pipe modification to accommodate dual-fuel operation, where the primary fuel is diesel (or biodiesel) and the secondary fuel is the producer gas. Also, compression ratio of the engine may need adjustment to optimize combustion efficiency for PG. Figure 3.1.2 illustrates the experimental installation of a downdraft gasifier unit in a lab, with Table 3.1.1(a

and b) listing its characteristics and working of its parts. To retain 1500 engine rpm, the compression ignition engine (CIE) incorporates a naturally aspirated, water-cooled, direct injection, eddy current load dynamometer, variable compression ratio (VCR) system, and auto governing system. Table 3.1.2 lists the details of an engine's setup. Engine Soft, a data acquisition system, was used to capture the parameters of engine combustion, fuel consumption, and performance on a computer. The AVL DIGAS 444 was utilized during an experimental investigation to evaluate engine emissions. Using test equipment, exhaust gas emission testing quantifies the gases emitted by an engine tailpipe. This is cantered on the notion of DOAS (Differential Optical Absorption Spectroscopy). The illumination is a xenon lamp, and the sensor is a simple spectrometer that reveals the delicate features of a specific wavelength range, or "window." Varying windows are used to distinguish distinct species of gases. The actual gas content can be found by mathematically processing the obtained spectra and comparing them to pre-recorded spectra of defined gases and defined ranges during the appropriate timeframe.

The exhaust gases are analysed using a probe inserted into the engine's tailpipe and a precise technique. Carbon monoxide (CO), carbon dioxide (CO_2), hydrocarbons (HC), and nitrogen oxides (NOx) are the four gases measured by the exhaust gas analyser. These measurements add up to a very exact approach to calculating the combustion efficiency of an engine. A Certified Reference Standard prepared according to ISO17025 is utilized to calibrate the device. Figure 3.1.3 depicts the lab view of the IC engine setup coupled with the PG mixing chamber. The air and gas flow rates were measured independently using a box-type orifice meter and a manometer. The specifications of the sound level meter are listed in Table 6. As per the sound level standards, the sound level meter was placed 1.5 m high above the ground level and 1 m rear sides of the variable compression ratio (VCR) engine exhaust, as shown in Figure 3.2.4. The specification of sound meter is tabulated in Table 3.1.3. A total of 48

experimental trial runs were carried out during the experimental campaign to complete the full examination.

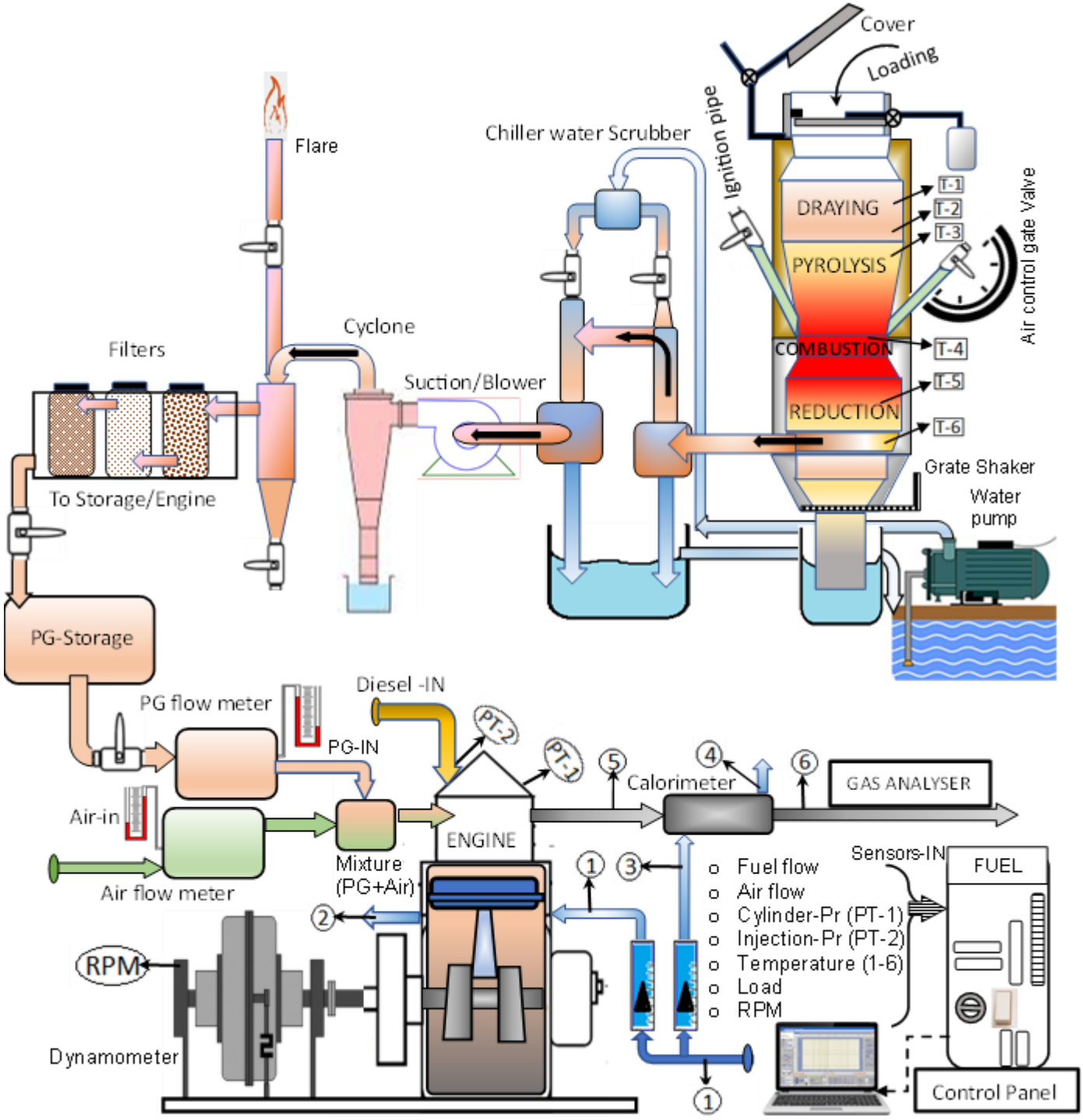

Figure 3.1.1. Block diagram representation of downdraft gasifier coupled with VCR engine

Figure 3.1.2. Gasifier with distinct integrated components for downdraft operation

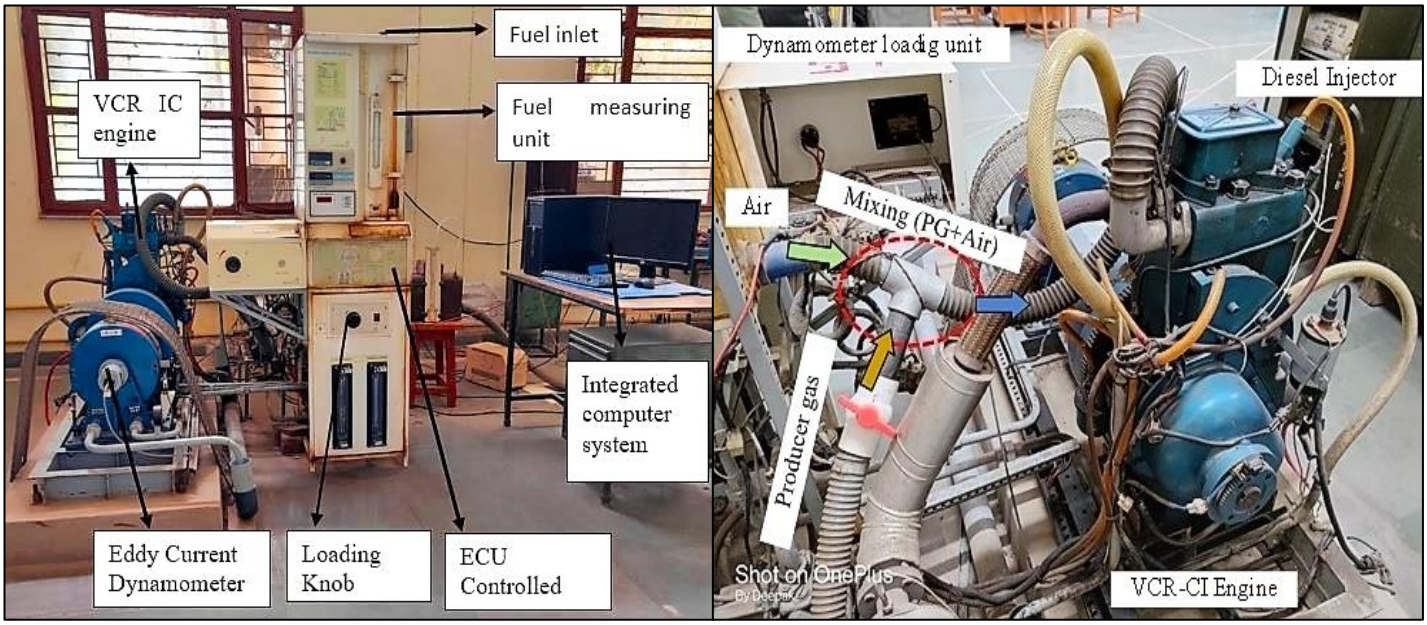

Figure 3.1.3. VCR – CI engine with integrated accessories and (air + PG) mixing point

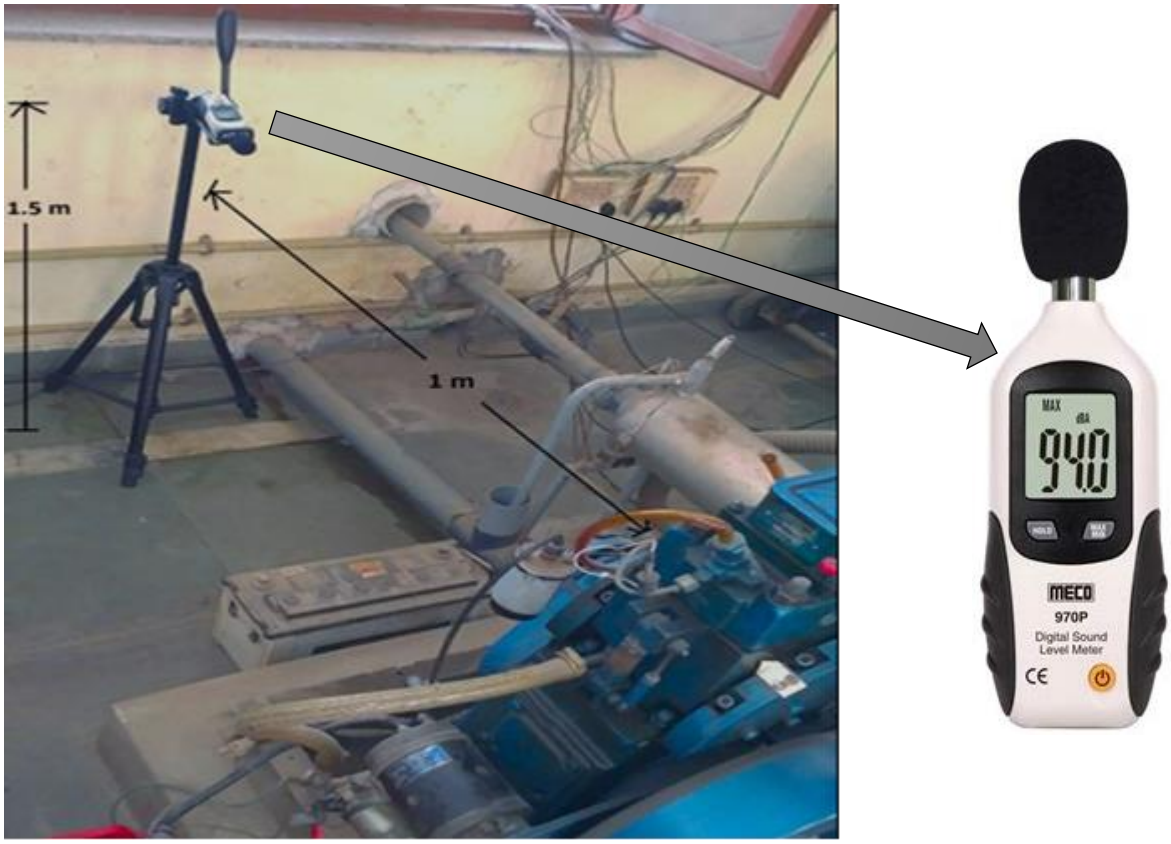

Figure 3.1.4. Photograph of Sound level meter placed at the engine exhaust

Table 3.1.1a. Technical details of biomass gasifier

Particulars	***Description***
Gasifier type	Downdraft
Gasifying agent	Air
Working pressure	Atmospheric
Rated fuel consumption	6 kg/hour
Rated power	14 kW
Rated gas flow	15 Nm^3/h
Temperature	800ºC to 900ºC
Air supply system	Two stainless steel pipes as nozzles
Hopper storage capacity	40kg
Feedstock feeding system	Manual loading
Discharge system	Grate and ash box
Gasifier nozzle open position (throttle)	***Gasification Equivalence ratio* (GER)**
100 % (Fully opened)	0.43
75 % (Quarterly closed)	0.36
50 % (Half opened)	0.24
25 % (Quarterly opened)	0.12

Table 3.1.1b. Gasifier Integrations

Accessories	Application
Air-control valve	To regulate the airflow
Blower	To maintain a steady flow of air
Water pump	For supplying water as a coolant and a filtering agent
Scrubber Cyclonic-separator	Primary filtration
Three-stage filtering system	Secondary filtration
Test flares facility	To confirm the flammability of released PG

Table 3.1.2. VCR engine descriptions

Setup units	Descriptions
Model	Kirloskar, 240PE
Engine type	VCR, Single cylinder, and 4-stroke CI Engine
Stroke length	11 cm
Bore	8.75 cm
Compression ratio	12:1 to 18:1
Cooling system	Water-cooled
Rated power	3.5 kW @ 1500 rpm
Dynamometer used	Eddy current (water cooling)
Rotameter	Engine cooling 40-400 LPH, calorimeter 25-250 LPH
Software	IC Enginesoft 9.0

Table 3.1.3. Specifications of Digital Sound Level Meter

Entity	Range
Frequency range (Hz)	31.5 ~ 8000
Measuring level range (dB)	35~130
Microphone	½ inch electret condenser microphone
Digital display	LCD, 3digits
Resolution	0.1 db
Accuracy	±1.5 db
Power supply	One 9V battery
Operation temperature	0~40ºC

3.1.2 Experimental procedure

A downdraft gasifier system was combined with a VCR compression engine, as shown in Figure 3.1.5, to study the engine's performance, fuel consumption, and emissions. The gasifier was loaded with 40 kg of mahua wood and briquette biomass. Thereafter, the air blower was turned on for the suction of air from the gasifier nozzle into the combustion zone and operated at gasification equivalence ratios ranging from 0.12 to 0.43. The magnitude of gasification ER corresponding to the different nozzle opening positions is shown in Table 3.1.1.

$$\text{Gasification Equivalence ratio (ER)} = \frac{\left(\frac{\text{Air}}{\text{Fuel}}\right)_{\text{actual}}}{\left(\frac{\text{Air}}{\text{Fuel}}\right)_{\text{stoichiometric}}} \quad (3.1.1)$$

$$\left(\frac{\text{Air}}{\text{Fuel}}\right)_{\text{stoichiometric}} = \left[\frac{1}{0.21}\left(1.866 \times \frac{\text{V}_\text{c}}{100} + 0.7 \times \frac{\text{V}_\text{s}}{100} + 5.55 \times \frac{\text{V}_\text{h}}{100} - 0.7 \times \frac{\text{V}_\text{o}}{100}\right)\right] \quad (3.1.2)$$

where V_c, V_s, V_h, and V_o are the volume percentage of carbon, sulfur, hydrogen, and oxygen in the biomass. The effects of actual to stoichiometric air-fuel ratio have significant importance on engine performance and emissions and have been discussed in the current study. Moreover, the effect of ER on combustible gases (CO_2/CO) was that higher ER leads to a higher air feed rate resulting in an increase in CO_2 while a decrease in CO gases. As ER increases from 0.35-0.43, CO decreases from 14.72% to 12.4%, as suggested by [139]. The flame was then kept near both the nozzle port for catching fire to the feedstock. Six thermocouples are attached at different zones of gasification reactions to measure the temperature along the height of the gasifier. Temperatures at different reaction zones were measured as the average temperature of T1 and T2 (drying), T3 (pyrolysis), T4 (oxidation/combustion), T5 (reduction zone), and T6 (grate) of the downdraft gasifier with six thermocouple positions installed at different locations along the gasification reaction zones. The maximum gasification temperature was around 600^{o}C at the inner surface of the gasifier shell near the oxidation zone. During the gasification

process, the feedstocks were consumed as fuel at a rate of 6 kg/h. After a certain time, the valve opened when the feedstock had been a little red hot, and the temperature reached around 600^{o}C and beyond at the oxidation reaction zone. PG was allowed to pass through a wet scrubber, cyclonic separator, and filtration zone to remove impurities. In the scrubbing and cooling section, PG passes through a water scrubber where the PG temperature reduces toward ambient temperature, and circulating water tries to remove the contaminants, tar, and soot particles that are soluble in water from the PG. However, the tar content of waste feed materials in fixed downdraft gasifier ranges from 0.02-4g/Nm^3 [140]. Besides, PG passed through a cyclone separator for further cleaning. Henceforward, the flammability of PG was frequently checked at the checkpoint until the testing flame changed its color and developed flare. It was observed that near 650^{o}C, the testing flame changed its color and developed a flare. After that, PG was allowed to pass through three chamber filtration units (rice husk, wood dust, and heavy cotton cloth) in a sinusoidal trajectory. Then, PG emerging out from the filtration unit, possessing a temperature in the range of 35-55^{o}C, was allowed to mix with air and enter the inlet section of the engine. The resulting PG was then used as fuel in the VCR engine in a dual-fuel mode, in which it was mixed with intake air. Tests were conducted with the VCR engine using pure diesel as fuel and with PG in the dual-fuel mode at different CRs (16-18), gasification equivalence ratios (0.12-0.43), engine BPs (0.1-3.5 kW), or engine load (0-12 kg), and blend (0-100 %). Data on engine performance, fuel consumption, and emissions were collected and analyzed using a data acquisition system 'IC Enginesoft' software which logged the collected data onto a computer display. The desktop view of IC Engine software can be seen in (Appendix A0). After collecting the data, RSM was utilized to optimize the independent input variables (gasification ERs, CRs, and engine loads), corresponding to the minimum fuel consumptions, sound intensity, and emissions, with maximization of engine BTE. However,

the experimental phase of a biomass gasification-IC engine study involves some challenges, ranging from fuel variability to technical complexities like-

- Producer gas composition varies with feedstocks and time span during the gasification process. This effects on possessing of the calorific value in the PG, which influences the performance of CI engine in dual fuel mode engine run.
- Biomass gasification produce tars and particulate matter, which can deposit on engine components and affect performance. Tar composition varies with time inside the gasifier. Also, it depends on variation in feedstock and its blends. Therefore, intermittently it effects the PG composition and its calorific value which influences the engine performances.
- During start of gasification process, CI engine cannot be coupled due to insufficient generation of flammable producer gases. Thus, achieving and maintaining stable operating conditions is crucial for reliable data collection.
- While feedstock gasification exhausts or ends, producer gas quality deteriorates. Thus, it marginally saves diesel fuel.

However, to address these challenges, a careful control of operating parameters, and statistical analysis of average data over time are employed for successfully conduction of gasifier-CI engine experiments. Moreover, a rigorous filtration unit is incorporated for tar and particulate matter filtration from biomass gasification and a permissible tar content of $0.1 g/m^3$ is maintained before an IC engine application.

Figure 3.1.5. Experimental setup of downdraft gasifier integrated CI engine

3.2 Economic methodology

This section is categorised into two sub-sections discussing the economic methodology of briquette production system from waste biomass. The subsequent sub-section discusses the economic methodology used for downdraft gasifier integrated CI engine.

3.2.1 Economic methodology of briquetting system

The economic analysis of briquetting system refers to evaluating the financial viability of producing briquettes from sugarcane bagasse pith (SBP) residues over 20 years. This type of analysis is essential in assessing the profitability of the production process and making informed decisions regarding the investments required. The study included the estimation of the initial capital cost required for the briquetting system. This consists of the cost of purchasing the machinery, equipment, and other materials needed to set up the system. To finance this cost, a 5-year loan term was assumed. The production unit currently produces 720 tons of briquettes from SBP annually. The economic parameters with different costs associated with the analysis are summarised in Table 3.2.1. The flow chart showing the steps involved in calculating the economic analysis of the briquette production system is shown in Figure 3.2.1. During the economic analysis, the net cash flow value for each year of simulation (t) was calculated using equation (3.2.1).

$$(\text{Net cash flow})_t = B_C B_P (1+i)^{t-1} - MC(1+j)^{t-1} - E_c E_P (1+k)^{t-1} - OS (1+n)^{t-1} - \text{Diesel}_c D_P (1+i)^{t-1} - PT (1+i)^{t-1} - B_{inder} B_P (1+i)^{t-1} - \text{Pack}_P (1+i)^{t-1} - LP \quad (3.2.1)$$

Where B_c is briquettes price (Rs./kg), Bp is annual briquettes production (kg), MC is Maintenance cost (Rs.), i is market inflation rate, j is maintenance cost inflation rate, Ec is the electrical energy used (kWh), Ep is electrical energy price (Rs./kWh), k is the electricity inflation rate, OS is operator's salaries (Rs.), Diesel_c is the quantity of diesel used (litre), Dp is diesel price (Rs./litre), PT is the properties taxes (Rs.), B_{inder} is the quantity of binder used (kg),

B_P is binder price (Rs./kg), Packp is the annual package price (Rs.), and LP is bank loan periodic payment (Rs.) which was expressed by equation (3.2.2).

$$\mathrm{LP} = \frac{\text{Inital capital cost}}{\frac{1}{\mathrm{m}}\left[1-\left(\frac{1}{1+\mathrm{m}}\right)^{\mathrm{N}}\right]} \tag{3.2.2}$$

Where m is bank loan inflation rate, N is fixed number of reimbursement years.

Furthermore, in this analysis, the profitability evaluation metrics employed are NPV and PI. NPV serves as a crucial tool for assessing whether a project or investment will yield a net profit or incur a loss. It is computed by summing up all the discounted future cash flows, as illustrated in equation (3.2.3). A positive NPV indicates a profitable outcome, whereas a negative NPV signifies a loss.

$$\mathrm{NPV} = \sum_{t=0}^{t=20} \frac{(\text{Net cash flow})_t}{(1+\text{discount})^t} \tag{3.2.3}$$

Where d is the discount rate over a year (t).

Additionally, the PI is a metric that expresses the correlation between the benefits and costs of an intended project. It is determined by taking the ratio of NPV to the initial capital cost, as shown in equation (3.2.4). A higher PI value indicates a more appealing project, making it more attractive for consideration.

$$\mathrm{PI} = \frac{\mathrm{NPV}}{\text{Inital capital cost}} \tag{3.2.4}$$

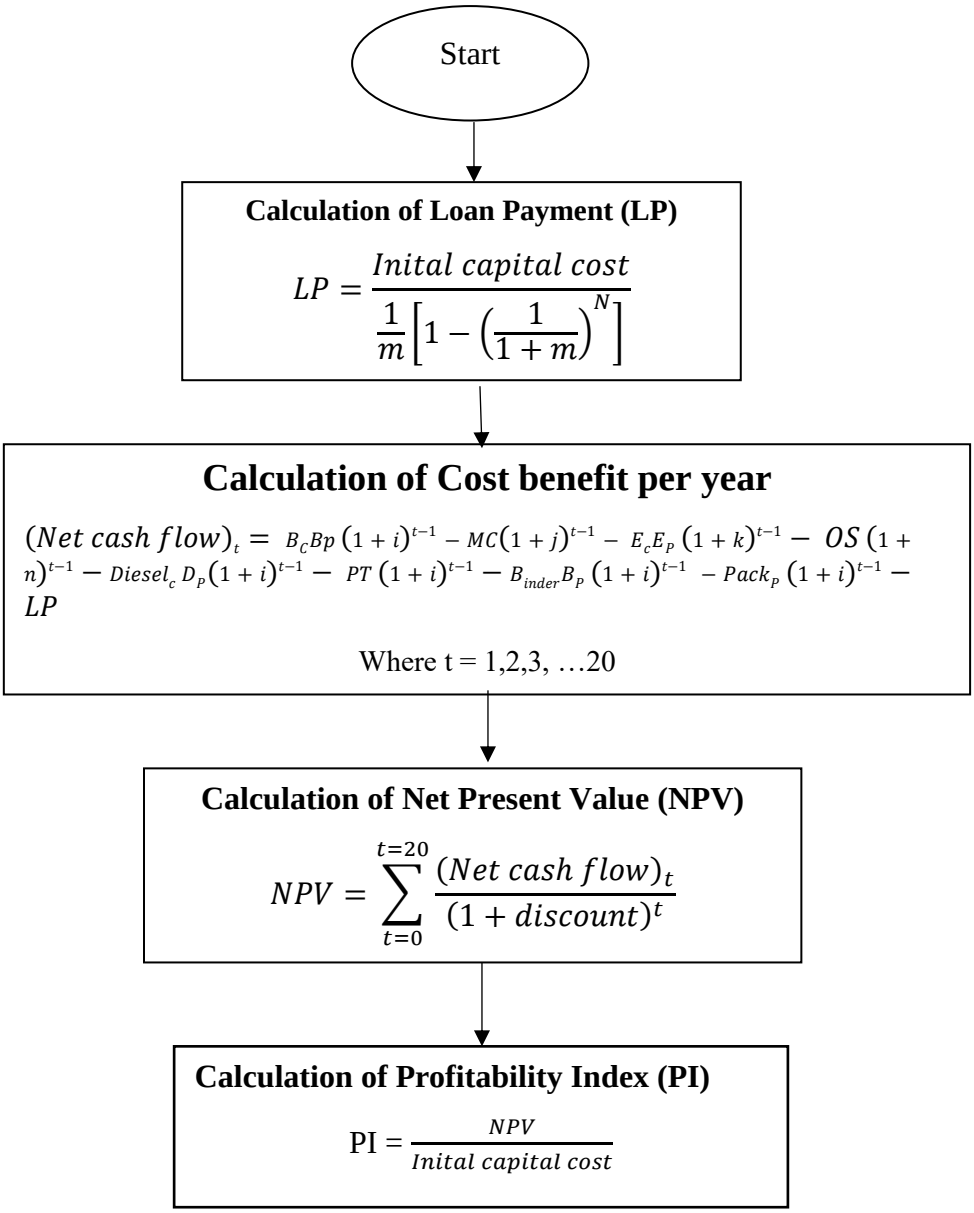

Figure 3.2.1. Flow chart involving economic analysis of Briquetting system

Table 3.2.1. Economic parameters of briquette plant

Parameters	**Value**
Initial capital cost	Rs. 25,00,000
Maintenance cost (MC)	Rs. 45,000
Maintenance cost inflation rate (j)	5%
Electricity price (E_p)	6.5 (Rs./kWh)
Binder price (B_p)	17 (Rs./kg)
Package price ($Pack_p$)	0.45 (Rs./kg of briquettes produced)
Diesel price (D_p)	90.08 (Rs./l)
Market price of SBP-briquettes (B_c)	12 (Rs./kg)
Fixed number of payback years (N)	5 years
Operator salary (OS)	50 (Rs./hour.person)
Electricity inflation rate (k)	0.1 %
Market inflation rate (i)	2.4 %
Bank loan interest rate (m)	7 %
Discount rate (d)	7 %
Operator salary inflation rate (n)	3 %

3.2.2 Economic methodology of gasification-engine system

The financial evaluation of a gasification-engine system involves the analysis of different parameters viz. capital cost, annual maintenance cost, fuel cost, levelised unit cost of electricity (LUCE), payback period is illustrated in the Figure 3.2.2. The formulation involved in calculating the economical parameters for a gasification-engine system is discussed below.

The annual electricity output (E_o) of the gasification-engine plant, which operates at an engine-rated capacity of (P), is reliant on the capacity utilization factor (CUF), a portion of power used by the auxiliary components of the plant (a), and the portion of losses experienced in the local power distribution grid (*l*). The estimation of the annual electricity output can be determined using the following formula-

$$E_0 = P(8760 \times CUF)(1 - a)(1 - l) \quad (3.2.5)$$

Moreover, the capital cost (AC_C) consists of costs of the gasification-engine plant (C_b), engine generator set (C_{eg}), civil works (C_w), and distribution network (C_d).

$$AC_C = C_b + C_{eg} + C_w + C_d \quad (3.2.6)$$

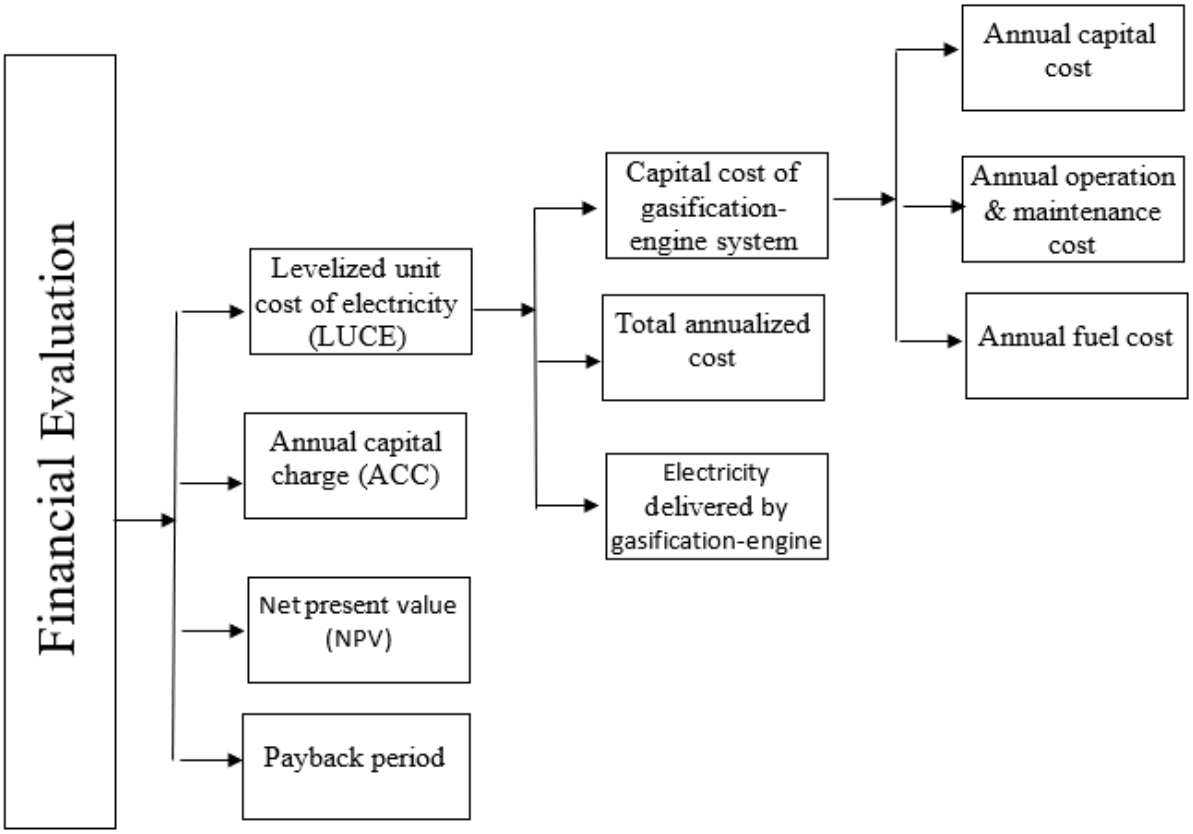

Figure 3.2.2. Flow chart involving economic analysis of Gasification-engine system

Further, Total annualized cost *(AC)* covers the capital expenses for various components of the gasification-engine system, annual operational and maintenance cost and the fuel expenditures was computed by applying appropriate capital recovery factors based on the expected lifespan of each component. Furthermore, the discount rate was factored in when assessing the capital costs of different subsystems. The contributions of annual capital cost (AC_C), annual operation

and maintenance cost ($AC_{O\&M}$), and annual cost of fuel (AC_F) towards the total annualized cost can be approximated using the following expressions [112]:

$$AC_C = C_g \times R_g + C_{eg} \times R_{eg} + C_{cw} \times R_{cw} + C_d \times R_d \quad (3.2.7)$$

where R_g, R_{cw}, R_d and R_{eg} represents the capital recovery factors for the gasifier, civil works, distribution network, and engine–generator set respectively. Considering a discount rate of '*D*', and useful life as '*t*', the capital recovery factor (R_f) can be expressed as [112];

$$R_f = D(1 + D)^t / (1 + D)^t - 1 \quad (3.2.8)$$

$$AC_{O\&M} = C_g \times n_g + Ceg \times n_{eg} + Cw \times n_w + C_d \times n_d + (8760 \times CUF \times n_l \times m) \quad (3.2.9)$$

where n_g ,n_{eg}, n_w and n_d represents the operation and maintenance costs of gasifier, engine genset, civil works, and distribution network respectively as fractions of their respective capital costs. *nl* and *m* represents the daily manpower wage and no of manpower respectively.

$$AC_F = 8760 \times CUF\ (c_{pf} \times s_{spfc} \times P + c_{bm} \times s_{sgfc} \times P) \quad (3.2.10)$$

where c_{pf} and c_{bm} represents the unit cost of pilot fuel (diesel) and biomass, respectively. s_{spfc} and s_{sgfc} represents the specific pilot fuel consumption and specific gaseous fuel consumption. Therefore, Total annualized cost can be represented as [112],

$$AC = ACC + AC_{O\&M} + AC_F \quad (3.2.11)$$

Additionally, LUCE represents a widely employed method in the financial assessment of decentralized power systems powered by renewable energy sources. LUCE can be described as the ratio between the total annualized cost (AC) [25] of the gasification-engine system and the annual electricity output generated by the gasification-engine system.

$$LUCE = AC / E_o \quad (3.2.12)$$

And, Annual capital charge (*ACC)* involves the process of converting the total capital charges of investment into annual equivalent charges and subsequently evaluating the project's viability by comparing it with annual net cash flow.

$$ACC = C_C \times i \,/\, 1 - (1 + i)^{-t} \tag{3.2.13}$$

where C_C and i are annual capital cost and rate of interest respectively. Moreover, the NPV, as elucidated in equation (3.2.3), is the approach used to ascertain the present worth of all cash flows over the project's operational lifespan, encompassing the initial capital outlay. And, the Payback period signifies the duration needed to recoup the initial investment allocated to a project.

$$Payback = AC_C / F \tag{3.2.14}$$

where, F is the net cash flow annually.

Moreover, some of the assumptions are also made for input parameters. Based on Samar et al. [112], a capacity utilization factor of 35% is assumed with electricity production of 10 h per day. The useful life of gasifier, DF engine, civil works, and distribution lines is assumed based on the different fabricating designs and materials as reported in different literatures. The cost of feed materials in the present study is assumed to be negligible as it is locally available in remote location, also the briquette feed materials are freely accessible from briquette manufacturing plant as the gasification-engine plant is established near the briquette manufacturing plant. The price of diesel is assumed as Rs. 90.08/l as on october 2023. The economic evaluation is made with/ without electricity distribution network, and the distance of electricity distribution is considered as 2 Km in present study.

3.3 Numerical Simulation methodology

So far as methodology is concerned to obtain the performance results and its analysis in SI engine, the direct experimental investigation requires a lot of manufacturing and time costs, therefore a wise approach is to predict the results by numerical simulation rather than conduction of experiments. Therefore, in this study, the SI engine performance simulation has been performed by quasi-dimensional (two-zone combustion) thermodynamic computational modeling. This deals with ordinary differential equations to simulate dynamic behavior during compression, combustion, and expansion stroke of closed power cycle SI engines. Simulation proceeds with compression stroke from the inlet valve closed, spark at the end of compression and sphere-like shape flame nucleus generation, then propagation of turbulent flame with two zones (burned and unburned) till the end of combustion, and to the expansion up to exhaust valve open. During the combustion phase, the flame front area and corresponding burned volume with the crank angle were calculated by flame front geometry till the end of combustion [141], and two-zone heat transfer from gas to the wall was computed using Annad's correlation [142]. The termination of burning inside the cylinder was hypothetically assumed when the volume of fresh charge ($V_{m)}$ becomes zero. During combustion, the formation of 12 product species (H_2O, H_2, OH, H, N_2, NO, N, CO_2, CO, O_2, O, and Ar) have been studied, and their equilibrium molar fractions are determined by the Newton-Raphson approach. Whereas CO and NO concentration for temperature and crank angle has been computed by applying a rate kinetics non-equilibrium model. The molar-specific heat and enthalpy of each mixture species have been calculated using polynomial interpolations with reference to temperature variation. The differential equation variables were determined using the fourth-order Runge-Kutta approach. In the quasi-dimensional thermodynamic mathematical model, the approximations and assumptions were captured with reference to Benson's [141] model which includes: (i) Gas flow into and out of the cylinder's crevices and heat transmission between burned and unburned

zones are disregarded, (ii) Homogenous mixture input of fuel and air, (iii) At all time, the pressure within the cylinder is uniform, (iv) Volume at flame reaction regions are negligible, (v) burned and unburned gas keeps constant local specific heat for, (vi) Negligible heat transfer between burned and the unburned zone, (vii) the unburned gas is frozen at ats original composition. Figure 3.3.1 shows the detailed process layout for engine simulation. The following modeling formulation was applied for the power cycle simulation of an internal combustion engine based on basic thermodynamic law:

3.3.1 Compression modeling

Compression starts from the inlet valve close (IVC) and the thermodynamic equation of state are [141], [143]:

The pressure in the cylinder of SI engine can be derived from the first law analysis. The cylinder pressure and product temperature versus crank angle is shown in equation (3.3.1&3.3.2)

$$\frac{dp}{d\theta}=\left(\frac{1}{V}\right)\left[\left(\frac{R}{c_v}\right)\left(\frac{dQ}{d\theta}\right)-\left(\frac{Pdv}{d\theta}\right)\left(\frac{R}{c_v}+1\right)\right] \quad \text{and} \quad \frac{dT_m}{d\theta}=T_m\left(\frac{1}{V}\frac{dV}{d\theta}+\frac{1}{P}\frac{dP}{d\theta}\right) \qquad (3.3.1\&3.3.2)$$

where P is the pressure inside the cylinder, θ is a crank angle, Q is heat releases, V is the cylinder volume and as a function of crank angle, given as

$$V=\frac{\pi}{4}D^2a_c\left[\left(1-\cos\theta\right)+\frac{L}{a_c}-\sqrt{\frac{L^2}{a_c^{\,2}}-\sin^2\theta}\right] \qquad (3.3.3a)$$

$$\frac{dV}{d\theta}=\frac{V_c}{2}(CR-1)\left[\left(\sin\theta\right)+\frac{\sin\theta\cos\theta}{\sqrt{\frac{L^2}{a_c^{\,2}}-\sin^2\theta}}\right] \qquad (3.3.3b)$$

where CR is the compression ratio, L is connecting rod length, a_c is a crank radius.

Using Annand's equation [142], the rate of heat transfer from the gas to the wall is computed:

$$\frac{q_h}{F} = \frac{a_c K_q}{d}(\mathrm{Re})^b (T_m - T_w) + c_c (T_m^4 - T_w^4) \tag{3.3.4}$$

where constants: $a_c = 0.4, b_c = 0.7$ and $c_c = -4.3\times10^{-9}$ F, d, K_q, R_e, T_m, and T_w are the area of cylinder walls, bore diameter, thermal conductivity, Reynolds number, Temperature of products, and wall temperature respectively. The work done by the cylinder contents on the moving piston is proceeded with:

$$\frac{dw}{d\theta} = \mathrm{p}\ \frac{dv}{d\theta} \tag{3.3.5}$$

As the compression process continues the variables increased by the fourth-order Runge-Kutta approach:

$$\mathrm{X_{n+1}} = \mathrm{X_n} + \frac{dX}{d\theta}\Delta\theta \tag{3.3.6}$$

where X is any variable, and $\frac{dX}{d\theta}\Delta\theta$ is the increment of variable X during a time step.

3.3.2 Combustion with two zones:

After an initial delay period [144], the two-zone combustion that consists of burned and unburned regions begins, and the subsequence flame continues to propagate. Figure 3.3.2 depicts the usual approach for the quasi-dimensional simulation of work and heat transfer between burned volume (V_p) and unburned volume (V_m). The burning rate and the states of a burned and unburned zone are determined by using the below equations [141], [143]:

$$\frac{dV}{d\alpha} = \frac{dV_m}{d\alpha} + \frac{dV_p}{d\alpha}\ ; = \left(\frac{V_p}{m_p} - \frac{V_m}{m_m}\right)\frac{dm_p}{d\alpha} + \frac{m_m R_m}{p}\ \frac{dT_m}{d\alpha} + \frac{m_p R_p}{p}\ \frac{dT_p}{d\alpha} - \frac{V}{p}\ \frac{dp}{d\alpha} \tag{3.3.7}$$

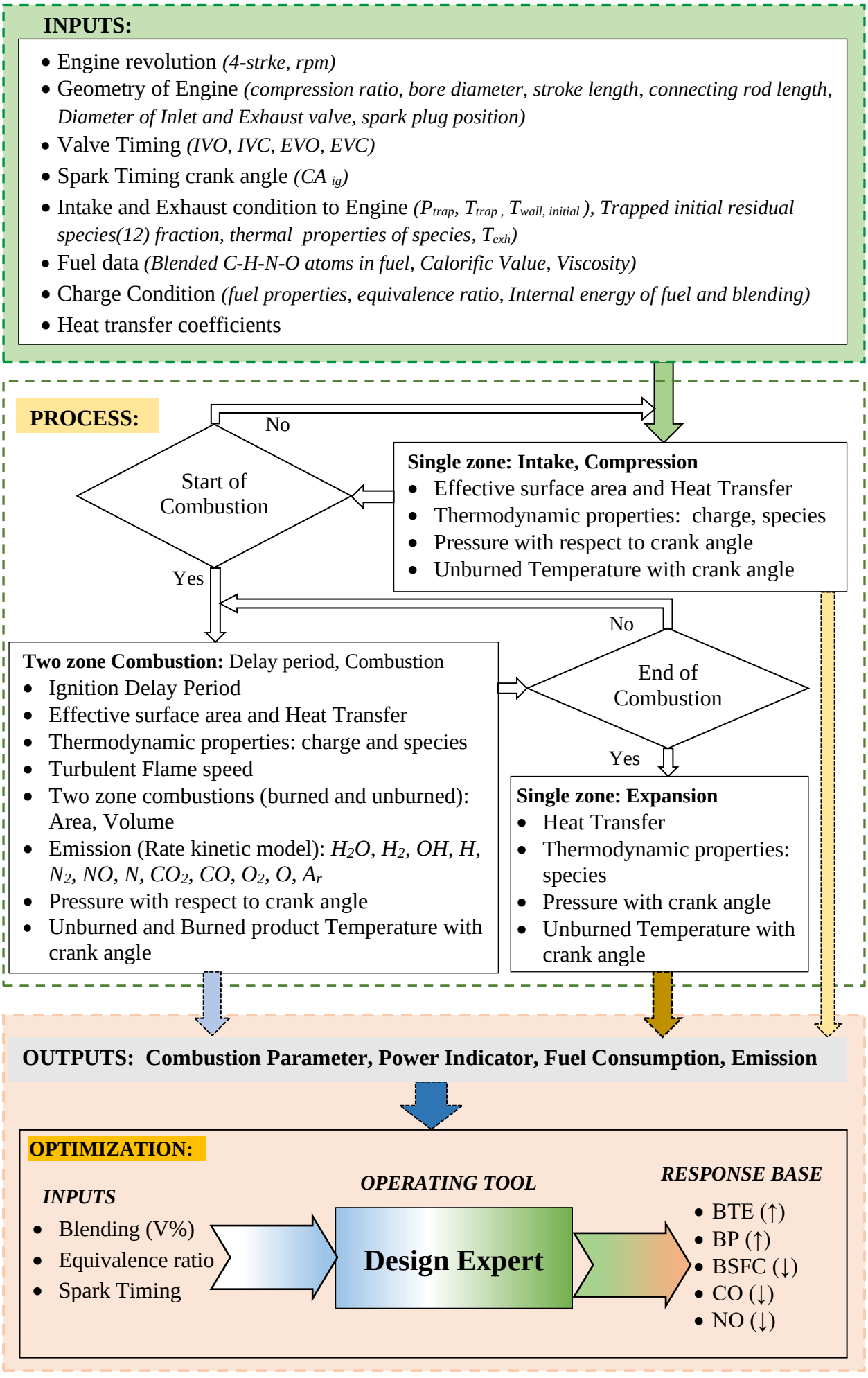

Figure 3.3.1. The Layout of the engine simulation and optimization process

$$\frac{dT_m}{d\alpha} = \frac{V_m}{m_m C_{p_m}}\left(\frac{dP}{d\alpha}\right) + \left(\frac{1}{m_m C_{p_m}}\right)\left(\frac{dQ_m}{d\alpha}\right); \tag{3.3.8}$$

where Q_m is heat transfer to the unburned mixture, assumed uniformly distributed throughout the mixture, and V_m is the specific volume of the mixture.

$$\frac{dT_p}{d\alpha} = \frac{p}{m_p R_p}\left[\frac{dV}{d\alpha} - \left(\frac{R_p T_p}{p} - \frac{R_m T_m}{p}\right)\frac{dm_p}{d\alpha} - \frac{R_m V_m}{p c_{pm}}\frac{dp}{d\alpha} - \frac{R_m}{p c_{pm}}\frac{dQ_m}{d\alpha} + \frac{Vdp}{pd\alpha}\right] \tag{3.3.9}$$

$$\frac{dp}{d\alpha} = \frac{\left(1+\frac{c_{v_m}}{R_p}\right)p\frac{dV}{d\alpha} + \left\{\left(u_p - u_m\right) - c_{v_p}\left(T_p - \frac{R_m}{R_p}T_m\right)\right\}\frac{dm_p}{d\alpha} + \left\{\frac{c_{v_m}}{c_{p_m}} - \frac{c_{v_p}}{R_p}\frac{R_m}{c_{p_m}}\right\}\frac{dQ_m}{d\alpha} - \frac{dQ}{d\alpha}}{\left[\frac{c_{v_p}}{c_{p_m}}\frac{R_m}{R_p}V_m - \frac{c_{v_m}}{c_{p_m}}V_m - \frac{c_{v_p}}{R_p}V\right]} \tag{3.3.10}$$

Burning rate: $\frac{dm_b}{dt} = A_f \rho_u u_T$ (3.3.11)

Where A_f, is the flame front area computed on the base of the geometrical model stated by Curto-Risso et al. [145], ρ_u is density and u_T is turbulent flame speed.

Turbulent flame speed: $u_T = u' + S_{L,PG+propane}$ (3.3.12)

turbulence intensity $u' = 0.5 S_p\left[1 - \frac{0.5(\theta - 180)}{45}\right]$ (3.3.13)

Table. 3.3.1 Specification of SI Engine

Particular	**Specification**
Gaseous Fuel Engine [97]:	Single Cylinder, 4-stroke, water-cooled gas SI engine
Displacement volume (L)	272 cc
Bore Diameter	82.0 mm
CR	9.0 -12.0
RPM	1500
Stroke	68.0 mm
Connecting rod length	136.5 mm

Particular	Specification
Equivalence ratio	Variable
Hydrogen fraction	0.55 (*validation*)
Blending	Variable
Spark timing	Variable

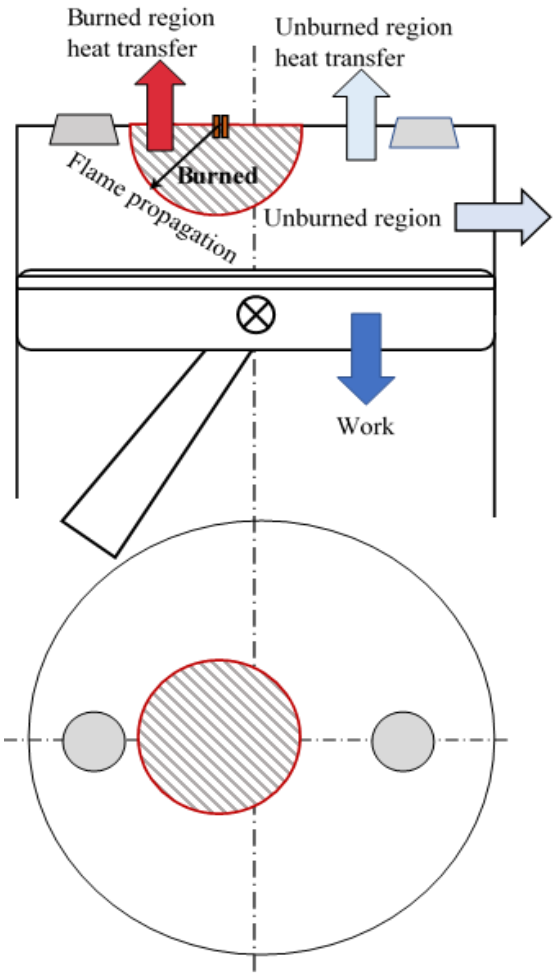

Figure 3.3.2. Combustion chamber (Quasi-dimensional) for engine simulation

The Laminar flame speed for duel fuel is computed by using Le Chatelier's Rule [146]

$$S_{L(PG+propane)}(\phi, x, T, P) = \left[\frac{x}{S_{PG+propane}(\phi, T, P)} + \frac{1-x}{S_{PG+propane}(\phi, T, P)} \right]^{-1} \quad (3.3.14)$$

Where $S_{l(PG)}$ and $S_{l(propane)}$ are the laminar burning velocity of Producer gas [99] and Propane [147]:

$$S_{l(PG)} = \left(S_{ref}\right)_{PG} \left(\frac{T_u}{T_{u,ref}}\right)^{\alpha} \left(\frac{P}{P_{ref}}\right)^{\beta} \quad , \tag{3.3.15}$$

$$S_{l(propane)} = \left(S_{ref}\right)_{propane} \left(\frac{T_u}{T_{ref}}\right)^{\alpha} \left(\frac{P}{P_{ref}}\right)^{\beta} \tag{3.3.16}$$

Where S_{ref} is the laminar burning velocity in m/s at $T_{u,\,ref}$ = 298 K, and P_{ref} = 1 atm, α, β, S_{erf} is depicted in Table 3.3.2.

Table 3.3.2. Value of constants

Value	**Producer gas**	**Propane**
α	2.0	2.18-0.8(Ø-1.0)
β	-0.4	-0.16 +0.22(Ø-1.0)
S_{ref}	0.56-0.827(Ø-1.186)^2	0.342-1.387(Ø-1.08)^2

The composition of producer gas from the Peach biomass gasification was adopted from the work of Tsiakmakis et al.[97]: 12.14%, 19.96%, 5.27%, 10.72%, and 51.91% for H_2, CO, CO_2, CH_4, and N_2. The dry HHV of peach biomass was 21.88 MJ/kg.

To calculate the internal energy of Peach-based producer gas, the polynomial coefficient J/kgmol for the composition has been taken from the reference [148].

$$U_{PG1} = CO_{2\,vol} \times (-0.48378 \times 10^5) + CO_{vol} \times (-0.1435 \times 10^5) + H_{2\,vol} \times (-0.98889 \times 10^3) + N_{2\,vol} \times (-0.10612 \times 10^4)\}8314 + [CH_{4\,vol} \times (-18.331 + 4.3)4183 \times 10^3)]$$

$$U_{PG2} = \{CO_{2\,vol} \times (0.24008 \times 10^{-1}) + CO_{vol} \times (0.371 \times 10^{-1}) + H_{2\,vol}) \times (0.30574 \times 10^{-1}) + N_{2\,vol} \times (0.36748 \times 10^{-1})\}8314 + [CH_{4\,vol} \times ((-0.29149 \times t)4183 \times 10^3 - 8314)]$$

$$U_{PG3} = \{CO_{2\,vol} \times (0.8735 \times 10^{-2}) + CO_{vol} \times (-0.1619 \times 10^{-2}) + H_{2\,vol} \times (0.26765 \times 10^{-2}) + N_{2\,vol} \times (-0.12082 \times 10^{-2})\} \frac{8314}{2} + [CH_{4\,vol} \times (\frac{26.327}{2} \times t^2 \times 4183 \times 10^3)]$$

$$U_{PG4} = \{CO_{2\,vol} \times (-0.6607 \times 10^{-5)} + CO_{vol} \times (0.36924 \times 10^{-5}) + H_{2\,vol} \times (-0.58099 \times 10^{-5}) + N_{2\,vol} \times (0.2324 \times 10^{-5})\} \frac{8314}{3} + \left[CH_{4\,vol} \times \left(\frac{-10.61}{3} \times t^3 \times 4183 \times 10^3 \right) \right]$$

$$U_{PG5} = \{CO_{2\,vol} \times (0.20022 \times 10^{-8}) + CO_{vol} \times (-0.2032 \times 10^{-8}) + H_{2\,vol} \times (0.5521 \times 10^{-8}) + N_{2\,vol} \times (-0.63218 \times 10^{-9})\} \frac{8314}{4} + \left[CH_{4\,vol} \times (\frac{1.5656}{4} \times t^4 \times 4183 \times 10^3) \right]$$

Where, $t = \frac{1}{1000}$

The polynomial Coeff. for internal Energy (J/kgmol) of propane(C_3H_8) has been taken from the reference [148] .

$U_{P1} = -0.7722 \times 10^8$

$U_{P2} = -14.532 \times 10^3$

$U_{P3} = 155.48$

$U_{P4} = 0.05447$

$U_{P5} = 8.4227 \times 10^{-6}$

Thus, the blended polynomial coefficient for internal Energy (J/kg-mol), where propane (C_3H_8) is blended in Producer gas, and *f* is the mole fraction of propane is as follows:

$$U_{Blend,i} = f.(U_{Pi})_{C_3H_8} + (1-f).(U_{PGi})_{PG}$$

Similarly, the internal energy of air and exhaust species was computed using polynomial coefficients [148] with the following equation.

$$C_V = (a_1 - 1)\,R + (a_2T + a_3T^2 + a_4T^3 + a_5T^4)\,\bar{R} \quad \text{J/kg mol} \tag{3.3.17}$$

$$\bar{h} = (a_1T + \frac{a_2}{2}\,T^2 + \frac{a_3}{3}\,T^3 + \frac{a_4}{4}\,T^4 + \frac{a_5}{5}\,T^5 + a_6)\,\bar{R} \quad \text{J/kg mol} \tag{3.3.18}$$

$$\bar{u} = ((a_1 - 1)T + \frac{a_2}{2}T^2 + \frac{a_3}{3}\,T^3 + \frac{a_4}{4}\,T^4 + \frac{a_5}{5}\,T^5 + a_6)\,\bar{R} \quad \text{J/Kg mol} \tag{3.3.19}$$

$$\bar{u}(T) = (u_1 + u_2T + u_3T^2 + u_4T^3 + u_5T^4 + u_6T^5) \quad \text{J/Kg mol} \tag{3.3.20}$$

Where; $u_1 = a_6\,\bar{R}$, $u_2 = (a_1 - 1)\,\bar{R}$, $u_3 = \frac{a_2}{2}\,\bar{R}$, $u_4 = \frac{a_3}{3}\,\bar{R}$, $u_5 = \frac{a_4}{4}\,\bar{R}$, $u_6 = \frac{a_5}{5}\,\bar{R}$

C_P *and* C_V is the specific heat capacity at constant pressure and constant volume respectively. $\bar{u}$ is internal energy, T is temperature, $\bar{h}$ is enthalpy, $\bar{R} = 8314\,J/kmolK$ is the universal gas constant and a_i (i =1, 2, 3, 4, 5, 6) are polynomial coefficients [148], and [149].

Molecular weight calculation:

$$W_{PG} = 28\times f_{CO} + 44\times f_{CO_2} + 16\times f_{CH_4} + 2\times f_{H_2} + 28\times f_{N_2}$$

Total blended Molecular weight

$$Wt_{(PG+\mathrm{Propane})} = W_{PG}\times (1-f) + W_{\mathrm{Propane}}\times f$$

Relationship between mass fraction (*x*) and mole fraction (*f*) [150];

$$x = \frac{f.MW_{C_3H_8}}{f.MW_{C_3H_8} + (1-f)MW_{PG}}$$

To calculate the calorific value per kg mass, the values of PG density are obtained using the calculation as follows [151]:

$$\rho_{PG} = [(f_1.\rho)_{CO} + (f_2.\rho)H_2 + (f_3.\rho)_{CH4} + (f_4.\rho)_{CO2} + (f_5.\rho)_{N_2}] \quad (kg/Nm^3)$$

Where the f_1 to f_5 are molar fractions of the compound of producer gas and the density of the compounds at NTP are ρCO =1.165 kg/Nm^3, ρH_2 = 0.089 kg/Nm^3, ρCH_4 = 0.668 kg/Nm^3, ρCO_2 = 1.842 kg/Nm^3, and ρN_2 = 1.165 kg/Nm^3.

The calorific value of PG was reference [97] equal to 3.97 MJ/Nm^3, 6.96 MJ/kg with a density equal to 1.167 kg/Nm^3 calculated by-

$$CV_{PG}\left(\frac{kJ}{kg}\right) = \frac{CV_{PG}\left(\frac{kJ}{Nm^3}\right)}{\rho_{PG}\left(\frac{kJ}{Nm^3}\right)}$$

Blended LHV (MJ/kg):

$$LHVt_{(PG+Propane)} = x.LHV_{C_3H_8} \times (1-f)x.LHV_{PG}$$

3.3.3 Species Formation

The reaction equation of dual fuel (Producer gas + Propane) and air for one mole of the total product is as below-

$$a\left[(1-f_{PG})C_3H_8 + f_{PG}PG\right] + \frac{a}{\varphi}\left[2(1-f_{PG}) + f_{PG}\right]\left(O_2 + \frac{78}{21}N_2 + \frac{1}{21}Ar\right) \rightarrow \sum_{i=1}^{12} x_i \qquad (3.3.21)$$

where '*f*' is the mole fraction of Producer gas in propane fuel.

The concentration of 12 species: H_2O, H_2, OH, H, N_2, NO, N, CO_2, CO, O_2, O, and Ar, are determined by atomic balance equations suggested by Benson et al. [141, 152]. However, the production of CO and NO in an engine is a non-equilibrium process. Therefore, the Rate kinetic model is used to simulate the CO and NO content proposed by Lavoie et al. [152, 153] and J. H. Horlock et al.[141] respectively.

3.3.4 General Performance Parameters:

Indicated work done: $\frac{dw}{d\alpha} = p\frac{dV}{d\alpha}$, $W_d = \int_{IVC}^{EVO}\left[P(\alpha)\ \frac{dV}{d\alpha}\right]d\alpha$ (3.3.22)

Indicated mean effective pressure: $IMEP(bar) = \frac{W_d(kJ)/100}{V_s(m^3)}$ (3.3.23)

Indicated power: $IP\ (kW) = \frac{W_d\ (kJ)}{120}\ N$; N is rpm (3.3.24)

Indicated thermal efficiency (ITE): $\eta_i = \frac{IP\ (kW)}{m\ (kg/s).\ CV(kJ/kg)}$ (3.3.25)

Indicated Specific fuel consumption: $ISFC\left(\frac{kg}{kWh}\right) = \frac{3600}{\eta_i\ .\ CV(kJ/kg)}$ (3.3.26)

Total motored friction mean effective pressure (TFMEP) [148]:

$$TFMEP(bar) = 0.97 + 0.15\left(\frac{N}{1000}\right) + 0.05\left(\frac{N}{1000}\right)^2 \quad (3.3.27)$$

Brake mean effective pressure (BMEP): $BMEP = IMEP - TFMEP$ (3.3.28)

Brake Power (BP): $BP = \frac{BMEP.\ V_s\ .\ N}{120}$ (3.3.29)

Brake Thermal Efficiency (BTE) $= \frac{BP*3600}{\dot{m}_f*C.V.}$ (3.3.30)

The general conversion from emission gas concentration to specific fuel consumption (g/kWh) for heavy duty vehicles is summarised as follows [154]:

$$CO\ (g/kWh) = 3.591\times 10^{-3} \times CO\ (ppm) \quad (3.3.31)$$

$$NO\ (g/kWh) = 6.636 \times 10^{-3} \times NOx\ (ppm) \quad (3.3.32)$$

$$HC\ (g\ kWh) = 2.002 \times 10^{-3} \times HC\ (ppm) \quad (3.3.33)$$

$$CO_2\ (g\ kWh) = 63.470 \times 10^{-3} \times CO_2\ (vol\%) \quad (3.3.34)$$

3.4 Optimization Methodology

Response Surface Methodology is a statistical and mathematical technique used to analyze the relationship between input parameters and output responses in order to optimize the response variables. It is commonly used in engineering to predict the outcomes of a system without conducting actual experiments. RSM is a valuable tool for the design of experiments and can save time and resources by reducing the need for actual experimental runs. The flow chart representing the techniques of RSM is depicted in Figure 3.4.1. This study optimizes the operating conditions (GER, CR, engine load, blend) of a dual fuel-CI engine running on (diesel-PG) from feedstocks (Coal, Briquette, Mahua wood, Coconut shell, and their different co-gasification blends) using RSM tool. RSM includes several steps. The first steps include opting for the input variables and their operating ranges and the response outputs (BSDC, BTE, Diesel saving, CO, HC, CO_2, and NOx). The chosen inputs are used to examine the influence of different feedstock-generated PG compositions. The current analysis investigates the influence of (Diesel-PG) blends on performance (BSDC, BTE, DS) and emission parameters (CO, HC, CO_2, and NOx) at varied input conditions. In the current study, RSM-based optimization strategy is used to enhance the engine performance and minimise the emissions. Secondly, choose an experimental design to compute the response. Central Composite Design (CCD) was

utilized because it offers accurate answers for second-order polynomials [155, 156]. A second-order quadratic equation well establishes the interrelationship between input variables and output response as [157, 158]:

$$R = C_0 + \sum_{i=1}^{n} C_i V_i + \sum_{i=1}^{n} C_{ii} V_i^2 + \sum_{i=1}^{n-1} \sum_{j-1}^{n} C_{ij} V_{ij} + \varphi \quad (3.4.1)$$

Where "*R"* is the response*, "V"* is the input variable and C_0, C_i, C_{ii}, *and* C_{ij} are the constant, linear, square, and 2-way interaction terms, respectively. *"n"* is no. of variables, and "φ" is random error.

Figure 3.4.2 shows the optimization method. Next, execute experiments, collect data, and test the model's correctness. The quadratic model optimizes linear and nonlinear relations. F-value, p-value, and Analysis of variance (ANOVA) findings were utilized to verify the fit and significance of performance and emission models. Residuals are expected minus actual data. F-value shows the relationship between a regression model's and residual's mean square value. Always increase its value for a structurally reliable model. A smaller p-value indicates better evidence and significance [156]. Therefore, p-values should be low. A higher F-value and a p-value of less than or equal to 0.05 both signal the importance of either an input parameter or the overall model. The F-value corresponds to the proportion of variation within and between groups. Model accuracy can be understood by evaluating the regression coefficient (R^2) and the adjusted regression coefficient (R^2_{adj}), both of which fall within the range of 0 to 100%. R^2 and R^2_{adj} values exceeding 90% suggest a highly accurate model. R^2 essentially measures the degree of fit, and for a model to be good, the discrepancy between R^2 and R^2_{adj} should be (<0.20). The relationship depicted in equation (2) and equation (3) is utilized to calculate the R^2, and R^2_{adj} respectively.

$$R^2 = 1 - \frac{\sum_{i=1}^{k} (r_{i,p} - r_m)^2}{\sum_{i=1}^{k} (r_i - r_m)^2} \quad (3.4.2)$$

$$R^2_{adj} = 1 - \frac{\sum_{i=1}^{k}(r_{i,p} - r_m)^2}{\sum_{i=1}^{k}(r_i - r_m)^2} \times \frac{(k-1)}{(k-n-1)} \tag{3.4.3}$$

where, k depicts the number of experiments; r_i, $r_{i,p,}$ and r_m depict experimental, predicted, and mean values, respectively.

Fourth, analyze the model with 3D graphs and determine optimum values. In the final stage, the model's desirability function is computed for the best process situations. However, The overall desirability function D is defined as the weighted geometric average of the individual desirability (d_i) according to the following equation [110, 159]:

$$D = (\prod (d_i^{w_i}))^{\frac{1}{W}} \tag{3.4.4}$$

If the importance is the same for each response, the composite desirability is:

$$D = (d_1 \times d_2 \times ..... \times d_n)^{\frac{1}{n}};$$

Where, d_i is the individual desirability for the i^{th} response, w_i is importance of the i^{th} response, W is $\sum w_i$ and n is the number of responses.

To maximise a response, the desirability is calculated as:

$$d_i = 0; y_i < L_i$$
$$d_i = ((y_i - L_i)/(T_i - L_i)^{r_i}; L_i \le y_i \le T_i$$
$$d_i = 1; y_i > T_i$$

And, to minimise a response, the desirability is calculated as:

$$d_i = 0; y_i > U_i$$
$$d_i = ((U_i - y_i)/(U_i - T_i)^{r_i}; T_i \le y_i \le U_i$$
$$d_i = 1; y_i < T_i$$

where, y_i is predicted value of i^{th} response; T_i is target value of i^{th} response; L_i is lowest acceptable value for i^{th} response; U_i is highest acceptable value for i^{th} response; D is the composite desirability; and r_i is weight of desirability function of i^{th} response.

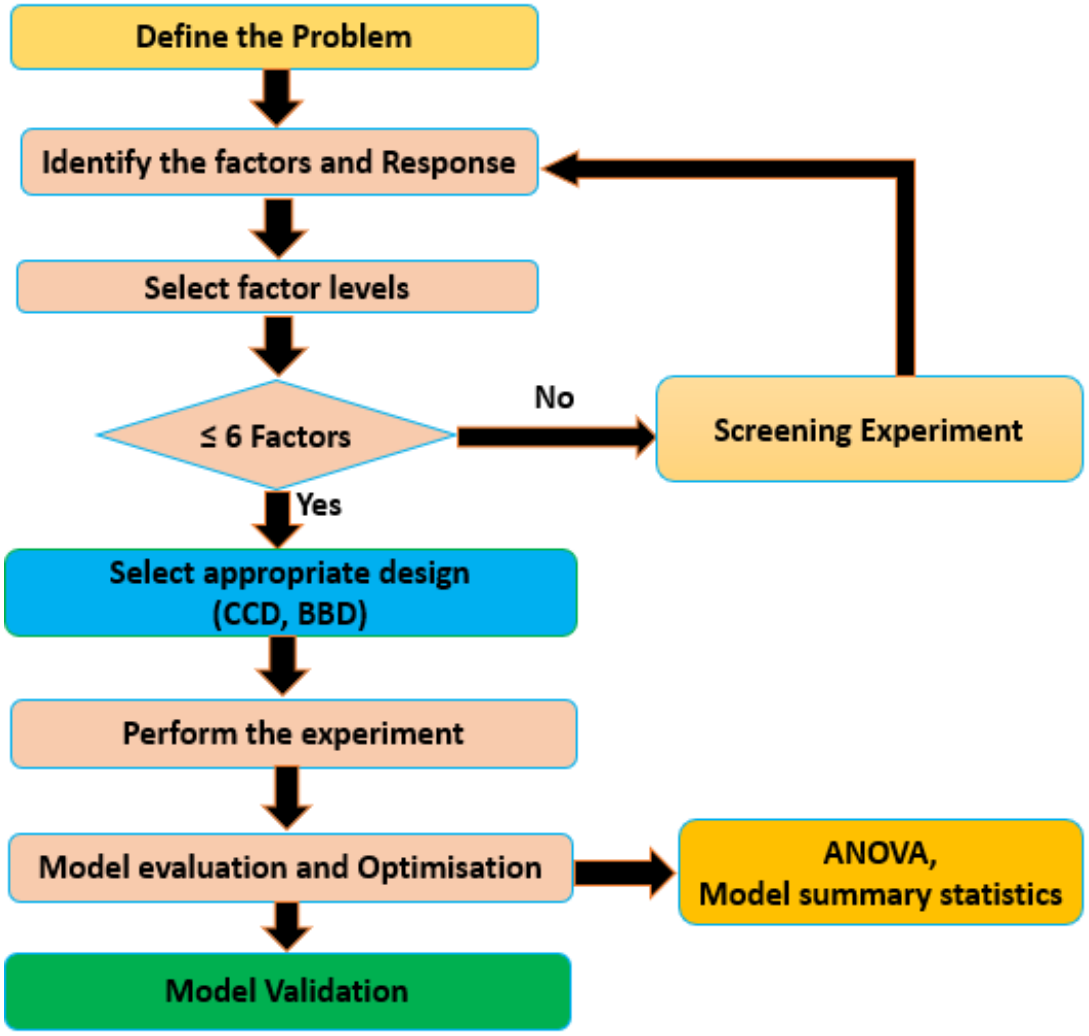

Figure 3.4.1. Flow chart of steps during RSM

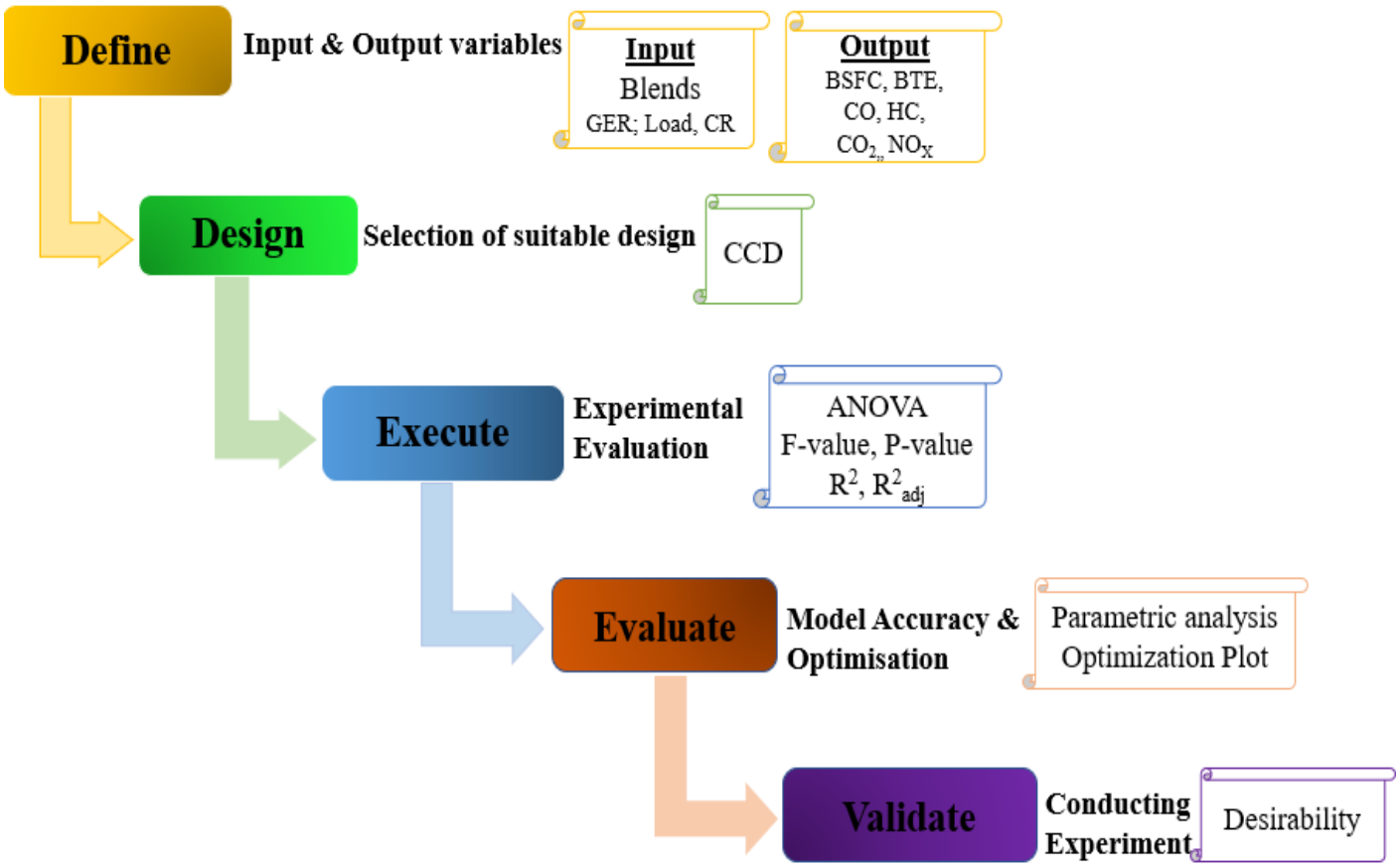

Figure 3.4.2. Flow chart of RSM-optimization